JOURNAL OF MATERIALS SCIENCE 30 (1995) 381–389

Moiré patterns and their application to the study of the growth of $YBa_2Cu_3O_{7-\delta}$ thin films

M. G. NORTON
Department of Mechanical and Materials Engineering, Washington State University, Pullman WA 99164, USA

C. B. CARTER
Department of Chemical Engineering and Materials Science, University of Minnesota, Minneapolis, MN 55455, USA

Very thin films of $YBa_2Cu_3O_{7-\delta}$ have been formed directly on specially prepared electron-transparent thin-foil substrates of MgO by pulsed-laser deposition and examined using transmission electron microscopy. The moiré fringe pattern visible in the electron micrographs has been used to provide information about film growth and the introduction of defects into the growing film. Individual domains, rotated about the [0 0 1] zone axis by small amounts, were detectable in the moiré fringe pattern by rotation of the fringes. In the case of small rotations, the fringe spacing varies only slightly. Individual domains rotated by large amounts, about the [0 0 1] zone axis, have been identified by the large variation produced in the moiré fringe spacing. The ability to identify domain rotation through examination of the moiré pattern is a very-fine-scale probe of local misorientations. Furthermore, these rotationally misaligned regions are formed directly at the film/substrate interface during the early stages of film growth. In some regions of the film, discontinuities in the moiré fringe pattern were observed. These discontinuities are indicative of growth-related defects, for example, threading dislocations. It was found that the number density of these defects was apparently reduced in films grown at higher substrate temperatures.

1. Introduction

Transmission electron microscopy (TEM) is an ideal technique for studies of thin-film growth processes. The high spatial resolution combined with the ability to obtain structural (electron diffraction) and chemical (X-ray analysis and electron energy loss spectroscopy) information, on a nanometre scale, make the electron microscope a valuable characterization tool. High-resolution electron microscopy (HREM) permits direct observation of grain boundary and defect structures in thin films. However, although HREM is a simple and direct means of obtaining important information on film growth, interpretation of the observations often requires the use of image simulations. The experimental constraints of HREM are that very thin specimens are needed. For plan-view imaging, this entails removing the substrate by, for example, ion milling to leave a region of free-standing film. Thus, for plan-view HREM studies, continuous films are required. Indirect imaging of growth-related defects by the use of moiré patterns offers a number of advantages both in terms of experimental constraints and on the necessary resolution of the electron microscope. In this present study, moiré fringe patterns have been used to examine structural defects in samples where the deposit was not a continuous film and was still on the substrate.

Moiré fringe patterns are formed in electron microscope images as a result of interference between diffracted beams from two overlapping crystals and, in the bright-field case, the direct beam [1, 2]. If the two crystals being considered are a deposited thin film and a single-crystal substrate, then information can be obtained about the orientation relationship between the two. The fringe patterns act as magnifiers of lattice imperfections and small deviations from perfect crystallographic orientation and symmetry.

A number of studies have used moiré patterns formed in electron microscope images to examine the growth of thin films [3–10]. Both *ex situ* and *in situ* deposition studies using electron-transparent substrates have provided some of the first direct information on the processes which occur during the initial stages of film growth. Metals grown on non-metallic substrate materials such as alkali halides (e.g. sodium chloride), molybdenite, graphite, or mica, were used in these cited studies. These materials were chosen because of their advantages in terms of ease of specimen preparation. Electron-transparent substrates of molybdenite and mica can be made by repeated clea-

0022–2461

ving, and alkali halides can be dissolved in water leaving a free-standing thin film which can be collected on a grid.

The experimental technique used in this present study employs the rationale of these earlier experiments, wherein an electron-transparent thin foil acts as the substrate material. In this study, the substrate material was (0 0 1)-oriented single-crystal MgO. Deposition of thin $YBa_2Cu_3O_{7-\delta}$ films was performed directly on to these substrates, which were then transferred straight from the deposition chamber to the electron microscope, thereby avoiding any possibility of defect introduction during post-deposition specimen preparation. The moiré fringe patterns produced in the electron micrographs were examined and used to provide information about film growth and the formation of growth-related defects.

2. Preparation techniques

The experimental details for preparing the thin-foil substrates have been reported elsewhere [11]. Briefly, the thin foil specimens were initially prepared using standard methods for the preparation of specimens for TEM analysis. Discs, 3 mm in diameter, were cored from a larger single-crystal substrate. These discs were mechanically polished and dimpled to produce a specimen thickness of $\sim 20\ \mu m$, then ion-milled to perforation using 5 kV Ar^+ ions. After ion-milling, the thin foils were chemically cleaned and annealed. The cleaning process is a multi-step process whereby any contamination resulting from ion-milling is removed. The high-temperature annealing produces a surface consisting of a series of well-defined terraces and steps. The annealing treatment for MgO was 1350 °C for 10 min.

Thin films of $YBa_2Cu_3O_{7-\delta}$ were prepared by pulsed-laser deposition (PLD) from a stoichiometric bulk target. The general method of film preparation has been described elsewhere [12]. The films were deposited by focusing a KrF ($\lambda = 248$ nm) excimer laser on to the target. The thin-foil substrates were mounted inside a single-crystal MgO holder through which a small hole had been drilled to facilitate passage of the ablated material. The thin-foil substrate and holder were mounted on copper foil on a Haynes-alloy substrate stage. The stage temperature was controlled to ± 1 °C and measured using an embedded thermocouple. The chamber was initially evacuated to better than 5 μ torr (1 torr = 133.322 Pa) and then equilibrated to 350–400 m torr oxygen. The stage temperature was maintained at 670 °C during deposition. Following deposition, the stage was cooled under atmospheric pressure of oxygen to room temperature. The laser was operated at a pulse repetition rate of 50 Hz and a fluence of $\sim 1\ J\,cm^{-2}$. The thickness of the films could be easily varied by changing the number of laser pulses.

The substrates were examined, by TEM, after film deposition using either a Jeol 1200EX operated at 120 kV or a Jeol 4000EX operated at 400 kV.

3. Observations and analysis

3.1. Spacing and rotation of the moiré pattern

Fig. 1 shows a high-resolution electron micrograph of a thin $YBa_2Cu_3O_{7-\delta}$ island on (0 0 1)-oriented MgO, where both the moiré pattern (illustrated by arrows) and the more finely spaced crystal lattice planes of the $YBa_2Cu_3O_{7-\delta}$ can be discerned. The moiré fringe spacing was measured from the image to be 2.05 nm; no difference in the orthogonal directions could be determined. The thickness of the island shown in Fig. 1 was estimated to be 12 nm. This value is based on an average deposition rate of 0.03 nm/pulse and a surface coverage of approximately 50% [12].

The island shown in Fig. 1 is oriented with its c-axis perpendicular to the film–substrate interface plane (c-axis oriented). Films produced under the deposition conditions described in Section 2 are almost exclusively c-axis oriented [12]. The orientation of individual grains can easily be determined in the electron microscope by their shape [13].

For the orthorhombic unit cell, the lattice parameters are $a = 0.382$ nm, $b = 0.389$ nm, and $c = 1.168$ nm [14]. For the tetragonal unit cell, the lattice parameters are $a = 0.385$ nm and $c = 1.170$ nm [15]. For MgO, the lattice parameter is $a = 0.421$ nm [16]. The predicted moiré fringe spacing, D_0, in the absence of any rotation, can be calculated from

$$D_0 = d_f d_s / |d_f - d_s| \quad (1)$$

where d_f and d_s are the lattice spacings of the interfering planes of the film and substrate, respectively. Thus, for c-axis oriented orthorhombic $YBa_2Cu_3O_{7-\delta}$ films on MgO, the predicted spacing of the moiré fringes is 2.06 and 2.56 nm for the (2 0 0) and (0 2 0) fringes, respectively. For c-axis oriented tetragonal films on MgO, the predicted moiré fringe spacing is 2.24 nm.

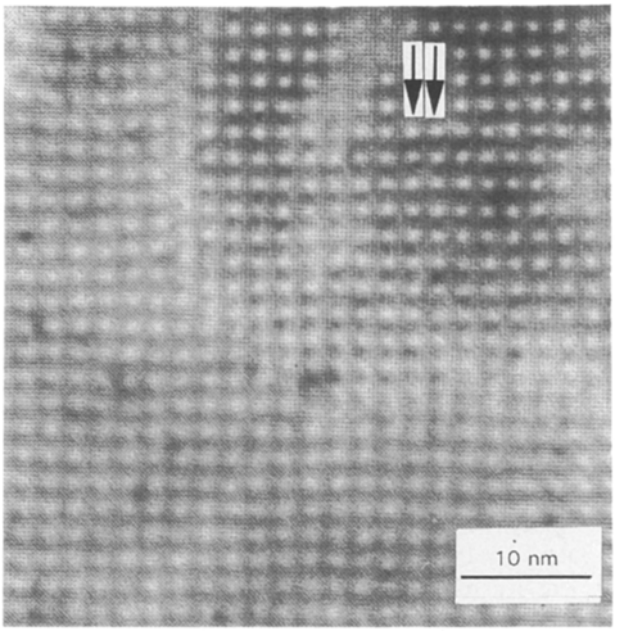

Figure 1 High resolution electron micrograph of a thin $YBa_2Cu_3O_{7-\delta}$ film on MgO. Both the lattice fringes and the moiré fringes are visible in the image.

The fact that no difference in the fringe spacing in the orthogonal directions was measured would suggest that these islands were tetragonal. However, examination of selected-area diffraction (SAD) patterns recorded from regions of the film shown in Fig. 1 clearly indicated a difference in the spacing of the (1 0 0) and (0 1 0) reflections arising from the film. The measurement of moiré fringe spacing may not be a good indication of orthorhombicity due to rotational effects which can alter the fringe spacing. Studies by other researchers have shown that $YBa_2Cu_3O_{7-\delta}$ thin films, of a similar thickness ($\sim$ 12 nm), deposited on MgO by off-axis magnetron sputtering were tetragonal [17]. In that study, tetragonality was determined by the use of grazing-incidence X-ray scattering. However, Streiffer *et al.* [17] note that there are no conclusive data on the precise film thickness at which orthorhombicity occurs, and that it can be expected to depend on substrate and deposition conditions.

Fig. 2 shows a low-magnification plan-view bright-field TEM image of a thin $YBa_2Cu_3O_{7-\delta}$ film on MgO recorded close to the [0 0 1] zone axis. The predominant moiré fringe spacing in this image varies from 2.15–2.35 nm; again no difference in the orthogonal directions could be determined. Five grains with different rotations about [0 0 1] are indicated in Fig. 2. The actual rotation of the grains can be determined by the rotation of the moiré pattern in these regions. Small rotations, θ, of the grains about the [0 0 1] zone axis produce rotations, ω, of the moiré fringes which are related by

$$\omega = d_f\theta/|d_f - d_s| \quad (2)$$

where the subscripts f and s again refer to the film and substrate, respectively. In addition to the moiré fringes being rotated, the fringe spacing decreases slightly to $D\omega$ which is given by

$$D_\omega \approx (d_f d_s/|d_f - d_s|)\cos\omega \quad (3)$$

Table I shows the moiré-fringe rotation and change in fringe spacing for several small rotations of the crystal lattice of the $YBa_2Cu_3O_{7-\delta}$. From Table I it can be seen that the rotation of the moiré fringes in this case ($YBa_2Cu_3O_{7-\delta}$/MgO) is larger by approximately an order of magnitude than the actual lattice rotation. The rotation of the moiré pattern visible in grain 1, in Fig. 2, is approximately 15° which would indicate that the actual rotation of the crystal lattice planes is 1.40°. Thus, the grain boundary shown in Fig. 3 between grains 1 and 2 is actually a low-angle grain boundary. Low-angle grain boundaries are frequently observed in $YBa_2Cu_3O_{7-\delta}$ thin films deposited on to substrates where there is a large lattice misfit, e.g. MgO and cubic ZrO_2 (e.g. [18, 19]).

Close examination of the moiré fringes in the vicinity of the grain boundary in Fig. 3, shows that they are curved: terminating fringes are also evident in the boundary region. Terminating moiré fringes indicate the presence of dislocations in one of the crystal lattices [1]. The predicted spacing of the dislocations, D_d, in the boundary calculated from Equation 4 is $\sim$ 16 nm, where $\boldsymbol{b}$ is the Burgers vector (0.385nm) and θ is the misorientation angle (1.40°) [20]

$$D_d = \boldsymbol{b}/\sin\theta \quad (4)$$

TABLE I Variations in rotation, ω and spacing, D_ω, of the moiré fringes for small rotations of the $YBa_2Cu_3O_{7-\delta}$ lattice, θ, calculated using Equations 2 and 3: d_f is taken to be 0.193 nm (an average of the (2 0 0) and (0 2 0) interplanar spacings for $YBa_2Cu_3O_{7-\delta}$ and d_s is 0.211 nm (the 2 0 0) spacing of MgO). Variations in the moiré fringe spacings in the *a* (D^a_ω) and *b* (D^b_ω) directions are also given

θ (deg)	ω (deg)	D_ω (nm)	D^a_ω (nm)	D^b_ω (nm)
0	0	2.278	2.060	2.561
0.25	2.68	2.276	2.060	2.558
0.50	5.36	2.268	2.053	2.550
0.75	8.04	2.256	2.042	2.536
1.00	10.72	2.238	2.026	2.516
1.25	13.40	2.216	2.006	2.491
1.50	16.08	2.189	1.981	2.461
1.75	18.76	2.157	1.952	2.425
2.00	21.44	2.120	1.919	2.384

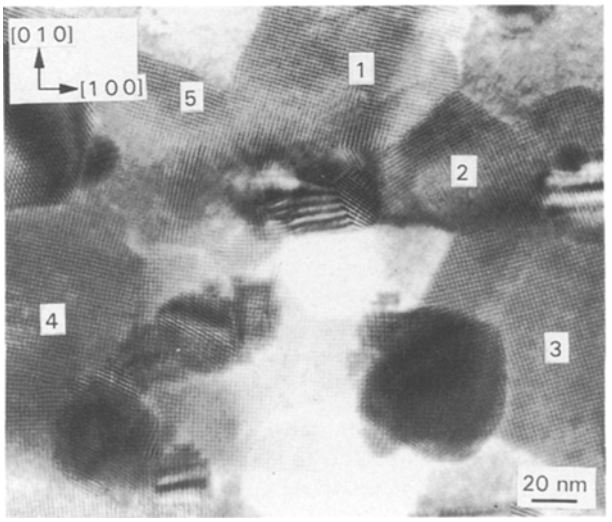

Figure 2 Bright field image showing moiré fringe pattern in coalesced grains.

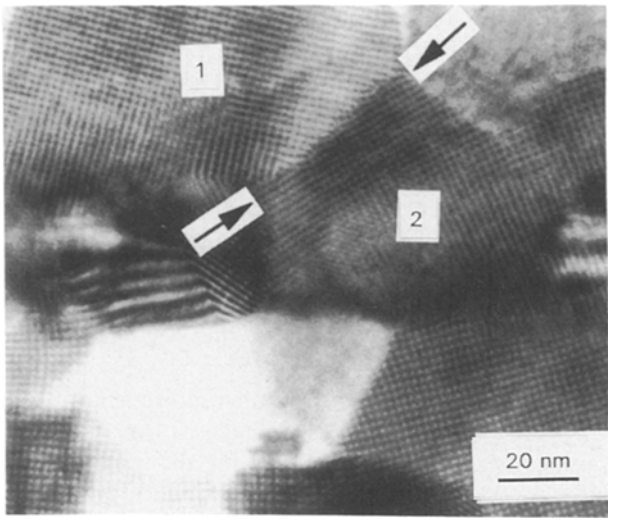

Figure 3 An enlarged image of part of figure 2, showing formation of a low-angle grain boundary.

This value for the dislocation spacing is in close agreement with the spacing of the terminating fringes measured in the boundary region between grains 1 and 2 in Fig. 3.

In some regions of the thin film, domains can be identified where the measured moiré fringe spacing is very different from the predominant fringe spacing observed earlier. In Fig. 4, three different sets of moiré fringe patterns are present, each with a different spacing. These domains have been identified and labelled as 1, 2, and 3, in Fig. 4. All the sets of moiré fringes are parallel – aligned in the $\langle 1\,0\,0 \rangle$ direction. The measured spacing of the moiré fringes in the three domains was: domain 1, 2.09 nm; domain 2, 0.09 nm; and domain 3, 1.90 nm. The dark circle around the image in Fig. 4 represents the position of the SAD aperture. A SAD pattern recorded from this area of the film is shown in Fig. 5a and the corresponding schematic in Fig. 5b. In the schematic drawing, reflections are denoted which correspond to regions of the film where the *a* and *b* crystal axes of the $YBa_2Cu_3O_{7-\delta}$ and the crystal axes of the MgO are aligned, as well as to regions where the $YBa_2Cu_3O_{7-\delta}$ lattice is rotated by 45°. Other reflections are visible in Fig. 5a which are much weaker, however, rotations of the $YBa_2Cu_3O_{7-\delta}$ lattice of 29° and 38° can be discerned. These rotations have been previously observed both by the authors [21] and by other researchers [22, 23].

The alignment of the three sets of moiré fringes in the $\langle 1\,0\,0 \rangle$ direction indicates that the interfering reflections, for the different sets of fringes, are aligned in the same direction. For parallel moiré fringes, the fringes always run perpendicular to $\Delta \boldsymbol{g}$, the line joining the operative $\boldsymbol{g}$ vectors for the two crystals [24]. In the case of the $\{2\,0\,0\}$ moiré fringes, interference is occurring between the $\{2\,0\,0\}$ reflections of the MgO and the corresponding reflections of the

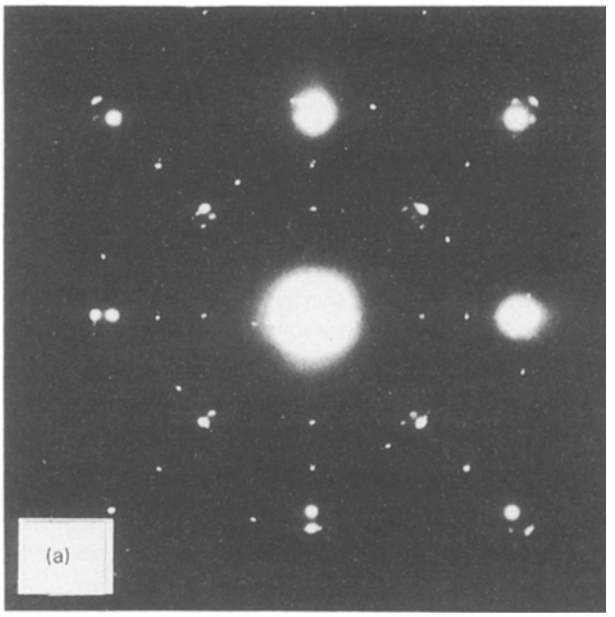

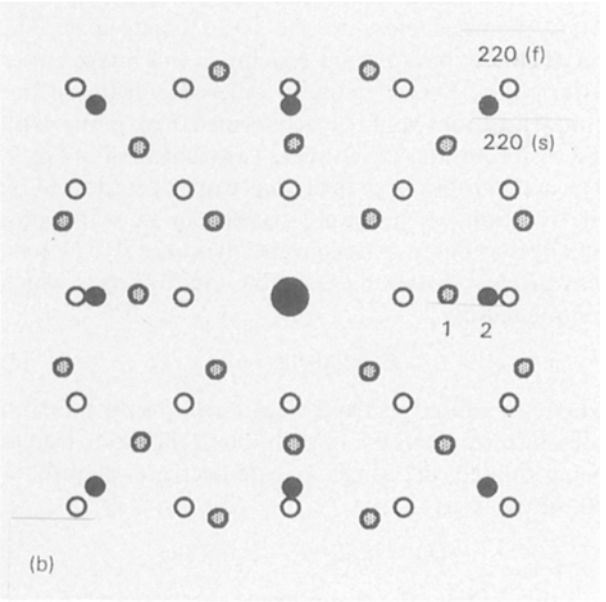

Figure 5 Selected-area diffraction pattern recorded from the area of film shown in Fig. 4 and corresponding schematic. Full circles are MgO; open circles $YBa_2Cu_3O_{7-\delta}$; shaded circles $YBa_2Cu_3O_{7-\delta}$ rotated by 45°. Reflections due to double diffraction have been omitted to aid clarity. The numbers 1 and 2 show two sets of reflections which produce one of the sets of moiré fringes shown in Fig. 4.

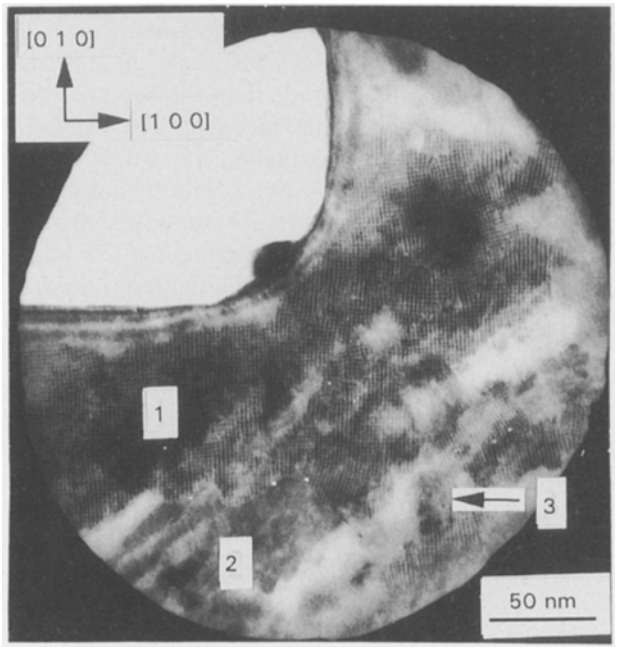

Figure 4 Bright-field image showing three domains, labelled 1, 2, and 3, each having a different moiré fringe spacing.

$YBa_2Cu_3O_{7-\delta}$. For domains rotated by 45°, the interference is between the $\{2\,0\,0\}$ reflections of the MgO and the $\{1\,1\,0\}$ reflections of the $YBa_2Cu_3O_{7-\delta}$. In the absence of rotation this would lead to a fringe spacing, D_0^{45}, calculated from Equation 1 where $d_f = 0.273$ nm and $d_s = 0.211$ nm, of $D_0^{45} = 0.926$ nm. For domains rotated by 26°, interference would be between the $\{2\,0\,0\}$ reflections of the MgO and the $\{1\,2\,0\}$ reflections arising from the $YBa_2Cu_3O_{7-\delta}$. Again, in the absence of any rotation, calculated from Equation 1 where $d_f = 0.173$ nm and $d_s = 0.211$ nm, the spacing of these fringes would be $D_0^{26} = 0.961$ nm. From the above observations, the three domains indicated in Fig. 4 can be assigned as follows: domain 1 corresponds to regions of the film where the *a*- and *b*-axes of

the film are aligned with the MgO crystal axes, domain 2 to regions of the film rotated by 45° and domain 3 is a small region of the film rotated by 26°.

Moiré fringes are thus very fine probes of the local crystallographic orientation of the film. Domain 3, in Fig. 4, is < 20 nm in diameter and therefore the orientation of this region could not be determined by SAD alone. By combining the information in the diffraction pattern with measurements of the spacing of the moiré fringe pattern and the fringe direction, the local orientation of different $YBa_2Cu_3O_{7-\delta}$ domains can be determined.

Fig. 6 shows another example where two sets of moiré fringe patterns having different spacings are visible. In region 1 the moiré fringe spacing is 1.97 nm (close to the predicted {2 0 0} moiré fringe spacing). In region 2 the fringe spacing is ~ 0.90 nm which would suggest a domain rotated by 45°. However, there is also a rotation of the moiré fringes between the two regions of 11°. In the same way that the fringe spacing was shown to vary with misorientation angle for the aligned grains, a similar situation occurs with these rotated grains. Table II shows the variation in fringe spacing and fringe rotation as a function of lattice rotation angle for a grain rotated away from an exact 45° misorientation. Thus, based on the data in Table II, it is concluded that region 2 in Fig. 6 is an area where the grain is rotated by 42.5° about the [0 0 1] zone axis. This orientation has been observed in $YBa_2Cu_3O_{7-\delta}$ films grown on cubic-ZrO_2 substrates by electron-beam evaporation and is close to the rotation for exact $\Sigma = 29$ special high-angle boundary in cubic or tetragonal materials [18].

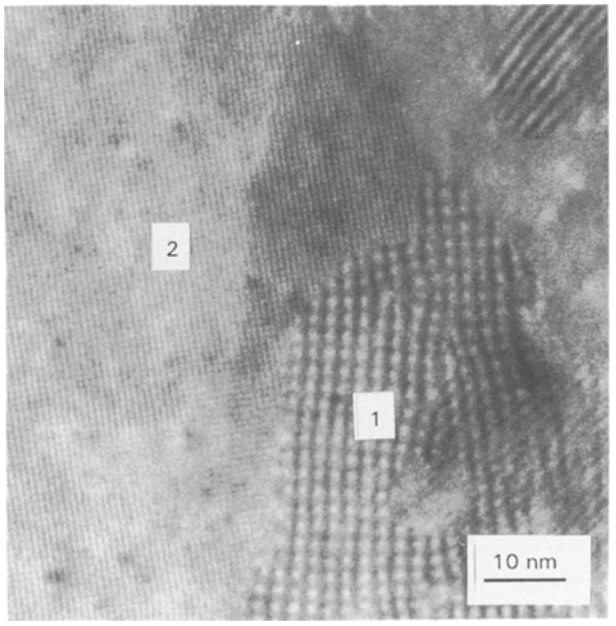

Figure 6 Bright-field image showing two sets of moiré fringes labelled 1 and 2.

TABLE II Variations in rotation, $\Delta\omega$, and spacing, D_ω^{45}, of the moiré fringes for small rotations of the $YBa_2Cu_3O_{7-\delta}$ lattice, $\Delta\theta$, away from 45° orientation calculated using Equations 2 and 3: d_f is taken to be 0.273 nm the {1 1 0} spacing of $YBa_2Cu_3O_{7-\delta}$ and d_s is 0.211 nm (the 2 0 0) spacing of MgO).

$\Delta\theta$ (deg)	$\Delta\omega$ (deg)	D_ω^{45} (nm)
0	0	0.926
0.25	1.1	0.926
0.50	2.2	0.925
0.75	3.3	0.924
1.00	4.4	0.923
1.25	5.5	0.922
1.50	6.6	0.920
1.75	7.7	0.918
2.00	8.8	0.915
2.25	9.9	0.912
2.50	11.0	0.909
2.75	12.1	0.905
3.0	13.2	0.902

3.2. Terminating moiré fringes

If a threading edge dislocation is present in the overlayer it will be visible as one or more terminating moiré fringes, depending on the magnitude of the Burgers vector and the reflection used to form the image. Many examples of areas where terminating fringes occur have been seen. The arrows in Fig. 7a indicate three areas where terminating fringes are visible. Fig. 7b–d are magnified images of each of these areas. At a threading [1 0 0] or [0 1 0] dislocation, two (2 0 0) or (0 2 0) moiré fringes will terminate. This situation is the one most commonly observed. However, single terminating fringes have also been found. Such single fringes indicate the presence of partial dislocations and thus widely extended stacking faults as have been observed, for example, by Tietz *et al.* [25]. Examples of double and single terminating fringes are shown in Fig. 7b.

Pinholes may be formed in the film as illustrated in Fig. 7c and d. So-called incipient dislocations [26] are often observed to be associated with such pinholes. When an excess of two moiré fringes terminate on one side of the pinhole it implies that one dislocation would have to be formed if the pinhole were to be eliminated but that may be locally energetically unfavourable [27]. In Fig. 7c it can be seen that six moiré fringes terminate on one side of the pinhole while four moiré fringes terminate on the other side. In some cases, more than two moiré fringes may terminate on the pinhole [28].

In Fig. 7d, the moiré fringes are seen to curve as they are followed away from the centre of the pinhole. The appearance of the moiré fringes in this area is suggestive of the presence of a disclination in the film. Again, if further film growth occurred it might be difficult to fill this pinhole. A tubular void would therefore remain in the film [27].

As mentioned in Section 2, the substrate temperature during deposition was 670 °C. Very thin films deposited at higher substrate temperatures (e.g. 750 °C) had microstructures which are very different from those observed for films deposited at 670 °C. Deposition at higher temperatures, for the same deposition times as used earlier, resulted in the formation of isolated islands, rather than the contiguous microstructure shown, for example, in Fig. 7a. The islands vary in size but were, in general, larger than

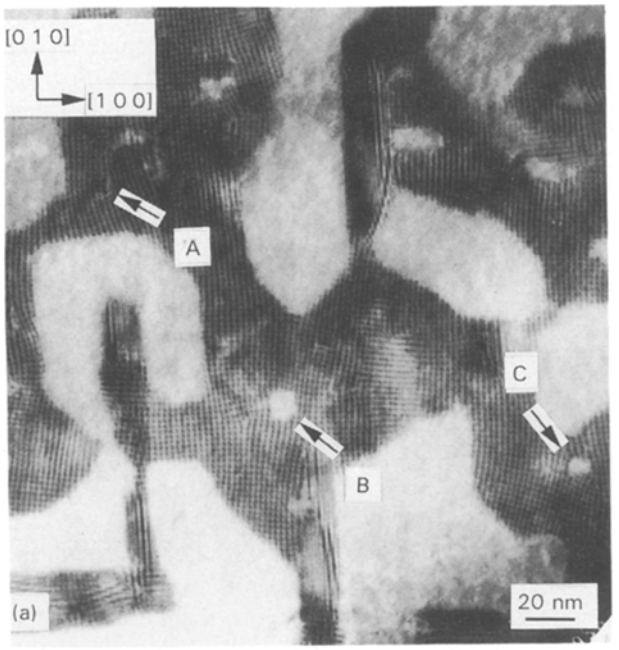

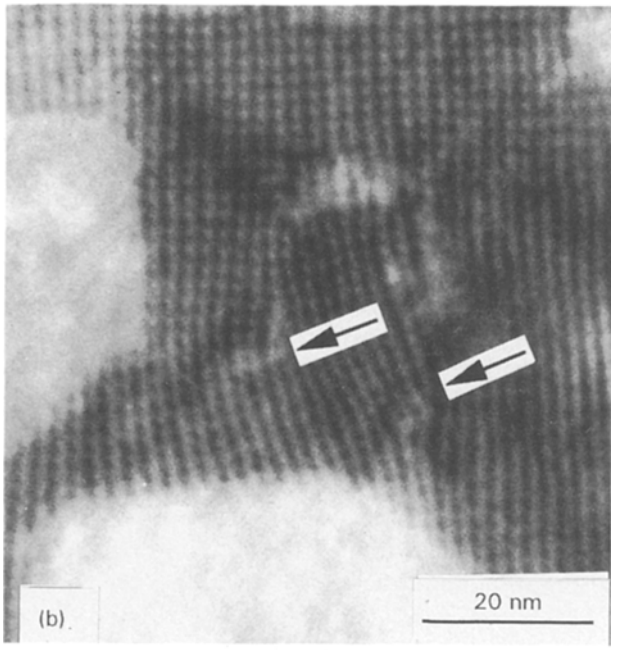

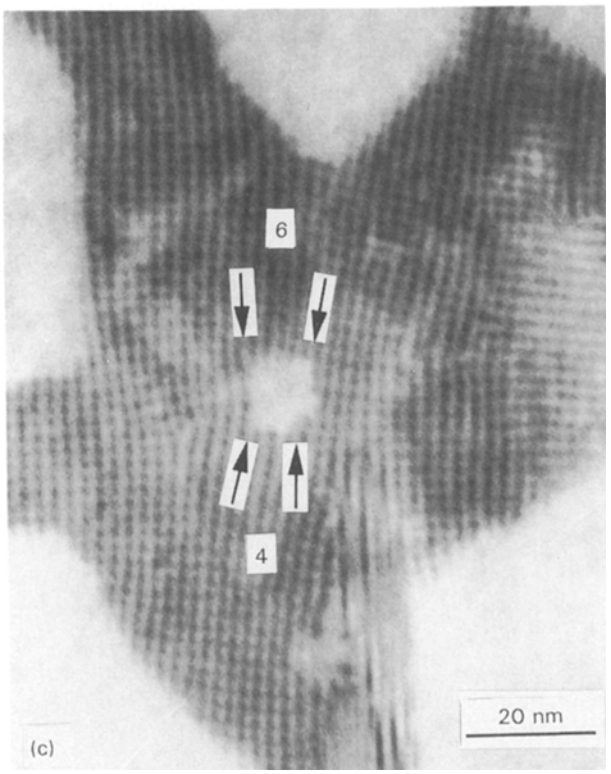

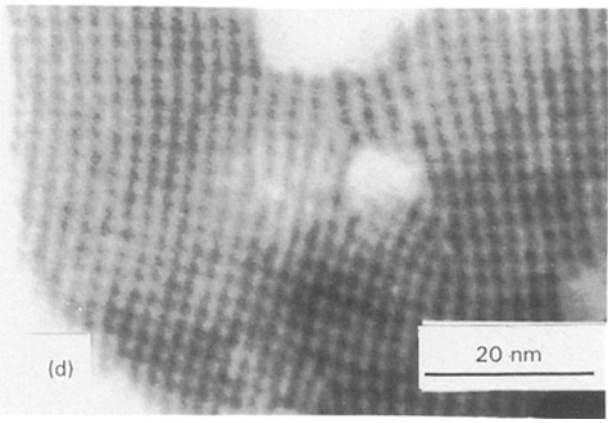

Figure 7(a) Bright-field image showing terminating moiré fringes. (b) Enlarged image of region A in (a). The arrows point to examples of terminating fringes. (c) Enlarged image of region B in (a). (d) Enlarged image of region C in (a).

those observed to form at lower substrate temperatures. The islands were again epitactic and oriented with their *c*-axes perpendicular to the film–substrate interface plane.

Fig. 8 shows a typical example of an isolated island produced on a MgO thin-foil substrate at a substrate temperature of 750 °C. Moiré fringes are visible in the image of the island and the moiré fringe spacing was measured to be 2.02 nm. This spacing is consistent with the spacing of the {2 0 0} moiré fringes discussed earlier. Close examination of the moiré fringe patterns shows that there are very few (in fact none could be

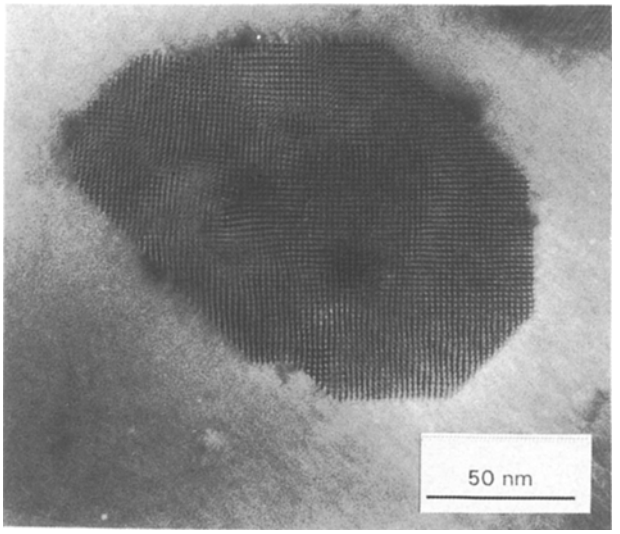

Figure 8 Bright-field image showing a typical example of an isolated island of $YBa_2Cu_3O_{7-\delta}$ on MgO produced at a substrate temperature of 750 °C.

seen in this particular island) internally terminating fringes in these islands; in contrast to the islands deposited at a substrate temperature of 670 °C.

4. Discussion

The presence of moiré fringes in the electron micrographs indicates a mismatch in the lattice spacings of the two crystals. If there is intimate contact between the film and the substrate, then either the heterojunction is incommensurate or an array of misfit dislocations is present at the interface. Cross-section TEM studies have demonstrated the intimate contact between $YBa_2Cu_3O_{7-\delta}$ films and MgO substrates (e.g. [25]). The spacings of the (2 0 0) and (0 2 0) moiré fringes are half those of the corresponding misfit dislocations. In an epitactically aligned *c*-axis oriented grain, the misfit will be accommodated by [1 0 0] and [0 1 0] misfit dislocations. The presence of misfit dislocations in thin $YBa_2Cu_3O_{7-\delta}$ films on MgO has been detected by ion-channelling studies [29] and direct evidence for the formation of a periodic array of interfacial dislocations in $YBa_2Cu_3O_{7-\delta}$ thin films on MgO has been obtained by HREM [22]. Recent work by Pennycook *et al.* has suggested that regions of both types of interface structure can occur [30].

In Fig. 2 the moiré-fringe spacing was determined to be between 2.15 and 2.35 nm, thus indicating that the spacing of the misfit dislocations would be between 4.30 and 4.70 nm. Values for the misfit dislocation spacing for a fully relaxed interface can be calculated using Equation 5, where b is the Burgers vector (calculated for the *a*-direction as 0.402 nm: $b = (a_f + a_s)/2$) and δ is the misfit (calculated for the *a*-direction as 10.2%: the misfit is given by $\delta = a_s - a_f/a_f$). For the case of orthorhombic $YBa_2Cu_3O_{7-\delta}$ on MgO the calculated misfit dislocation spacings are $D_{(1\,0\,0)} = 3.94$ nm and $D_{(0\,1\,0)} = 4.82$ nm

$$D = \boldsymbol{b}/\delta \tag{5}$$

The close agreement between the calculated and measured values indicates that strain relief is almost complete in these films. A further measure of the extent of strain relief can be obtained from the electron diffraction patterns. In some regions of the film, the moiré fringes did appear wavy, which would suggest that not all the strain had been relieved locally by the formation of misfit dislocations.

Because of the magnification factor in the moiré fringe patterns, they are very sensitive probes for examination of structural defects (e.g. [4]). In fact, artificial moiré patterns have been generated by overlaying perfect lattice images on lattice images of defect regions to generate moiré fringe patterns which reveal details concerning the strain fields around precipitates [31]. In the present study, moiré fringe patterns have been demonstrated to be a useful technique for determining the presence of rotationally misaligned domains in a growing film. For small rotations there is only a small change in the moiré fringe spacing, but an order of magnitude change in the rotation of the moiré fringe patterns. For large misorientations, such as 45°, there is a larger change in the fringe spacing associated with the rotational misalignment. Thus the orientation of nanometre sized domains can be readily identified, even when it may be difficult to obtain electron diffraction patterns from these individual regions. Furthermore, this study clearly demonstrates that these rotationally misaligned regions are formed directly at the film/substrate interface during the early stages of film growth.

Threading dislocations are another type of growth-related defect observed in thin $YBa_2Cu_3O_{7-\delta}$ films on MgO. The possible mechanisms for introducing dislocations during film growth have been discussed by Pashley [26]. In Fig. 7b it is believed that the accommodation of rotational displacements between agglomerating islands, that are close to the exact epitactic orientation, has lead to the formation of the threading dislocation. The fringes around the dislocation are clearly rotationally misaligned with respect to each other. Direct determination of the direction of the Burgers vectors of these dislocations from the moiré fringe pattern is not possible because of the large rotation of the moiré fringes. However, because only small changes in the fringe spacing occur with the rotation it is possible to determine the magnitude of the Burgers vector providing the contributing reflections are known. By counting the number of terminating moiré fringes, the density of threading dislocations which occur in thin films of $YBa_2Cu_3O_{7-\delta}$ on MgO due to island coalescence has been estimated by Streiffer *et al.* to be 10^{11} dislocations cm^{-3} [17].

For samples produced in this study, the propagation of substrate defects into the growing film is not a likely source of the observed threading dislocations. The high-temperature annealing of the substrates prior to film deposition removes any damage resulting from the polishing and dimpling procedures [11]. In addition, all the substrates were examined by TEM prior to film growth and in none of the cases reported in this paper was there any evidence for dislocations or other forms of microstructural defects in the substrates.

Incipient dislocations, associated with pinholes in the film, have been observed in other studies of thin film growth by the examination of moiré fringe patterns (e.g. [3, 8]). Pashley [26] postulated that plastic deformation of the film at the edge of the pinhole was the most probable mechanism for the formation of multiple incipient dislocations observed in gold deposits grown on molybdenum disulphide. For the $YBa_2Cu_3O_{7-\delta}$ on MgO case, the mechanism for the formation of these pinholes is not yet understood. However, it is clear that the pinholes form during the early stages of the film-growth process. It is not known how many are filled in during further film growth, but certainly pinholes have been observed in thicker $YBa_2Cu_3O_{7-\delta}$ films (e.g. [32]). Another possible source of pinholes in $YBa_2Cu_3O_{7-\delta}$ films is the feature shown in Fig. 7d which from the appearance of the moiré fringe pattern appears to be a disclination. Again, the moiré fringe patterns provide no information on the origin of these defects but do provide a means of observing them. The moiré fringe pattern

seen around the pinhole shown in Fig. 7d is not as common as the situation shown in Fig. 7c.

Moiré fringe patterns were used to examine island formation in films deposited at higher substrate temperatures. The islands were generally much larger than those observed for growth at the lower substrate temperatures used in this study and in other studies [33]. This feature is not surprising because the surface mobility of the ablated species would be expected to be greater at the higher substrate temperatures. The island shown in Fig. 8 is clearly faceted, this faceting is parallel to low-index planes as has been discussed elsewhere [33]. Within the individual facet planes, smaller microfacets are frequently observed; indicative of a ledge growth mechanism. The faceting of all the islands is parallel to the same low-index planes and hence it might be expected that when two islands coalesced there would be no rotational misorientation between them, thus reducing the number of threading dislocations in the film.

It is interesting to compare the results of this present study with other studies which have examined the growth of $YBa_2Cu_3O_{7-\delta}$ films using scanning tunnelling microscopy (STM) (e.g. [34, 35]. In both these studies, the authors found differences in the morphology of $YBa_2Cu_3O_{7-\delta}$ films grown at different substrate temperatures. The STM studies demonstrated that at higher substrate temperatures the screw dislocation growth mode may be suppressed. For example, Schlom *et al.* [34] found a decrease in the screw dislocation density as the substrate temperature was raised, and Norton *et al.* [35] found that at high substrate temperatures the spiral structures, associated with the presence of screw dislocations, were absent. These STM results appear, at least qualitatively, to agree with the present TEM study where differences in the island structure and apparent growth mechanism may be occurring at different substrate temperatures.

5. Conclusion

In conclusion, moiré fringe patterns in electron microscope images of $YBa_2Cu_3O_{7-\delta}$ on MgO have been used to examine the early stages of the film-growth process. The fringe patterns act as magnifiers of lattice imperfections and rotational misalignments in the film. They also allow the detection of small localized regions of the film which are not in perfect crystallographic alignment or where high-angle grain boundaries are present. Many of the microstructural features which have been observed to form during the early stages of the growth process and are also observed in thicker films; these features include pinholes, small-angle grain boundaries and special high-angle grain boundaries. This study has demonstrated an effect of substrate temperature on the perfection of thin films because it has shown that islands produced at higher substrate temperatures have apparently lower defect densities.

Acknowledgements

This work was supported, in part, by the Consortium for Superconducting Electronics (MDA 972–90C –0021). The authors would like to thank Dr Stuart McKernan for many helpful discussions.

References

1. P. B. HIRSCH, A. HOWIE, R. B. NICHOLSON, D. W. PASHLEY and M. J. WHELAN, in "Electron Microscopy of Thin Crystals" (Kreiger, Malabar, 1975) pp. 353–87.
2. J. W. MENTER, *Adv. Phys.* **7** (1958) 328.
3. G. A. BASSETT and D. W. PASHLEY, *J. Inst. Metals* **87** (1958–9) 449.
4. G. A. BASSETT, J. W. MENTER and D. W. PASHLEY, *Proc. R. Soc. A* **246** (1958) 345.
5. D. W. PASHLEY, M. J. STOWELL, M. H. JACOBS and T. J. LAW, *Philos. Mag.* **10** (1964) 127.
6. J. W. MATTHEWS and K. ISEBECK, *ibid.* **8** (1963) 469.
7. J. W. MATTHEWS, *ibid.* **7** (1962) 915.
8. Y. KAMIYA and R. UYEDA, *Acta. Crystallogr.* **14** (1961) 70.
9. G. HONJO and K. YAGI, in "Current Topics in Materials Science", edited by E. Kaldis, Vol. **6** (North Holland Publishing Co; New York NY, 1980) p. 197.
10. R. VINCENT, *Philos. Mag.* **19** (1969) 1127.
11. M. G. NORTON, S. R. SUMMERFELT and C. B. CARTER, *Appl. Phys. Lett.* **56** (1990) 2246.
12. S. E. RUSSEK, B. H. MOECKLY, R. A. BUHRMAN, J. T. McWHIRTER, A. J. SIEVERS, M. G. NORTON, L. A. TIETZ and C. B. CARTER, in "High Temperature Superconductors: Fundamental Properties and Novel Materials Processing", edited by J. Narayan, C. W. Chu, L. F. Schneemeyer, and D. K. Christen. Materials Research Society Symposium Proceedings, Vol. **169** (MRS, Pittsburgh PA, 1989) p. 455.
13. M. G. NORTON, S. McKERNAN and C. B. CARTER, *Philos. Mag. Lett.* **62** (1990) 77.
14. R. J. CAVA, B. BATLOGG, R. B. VAN DOVER, D. W. MURPHY, S. SUNSHINE, T. SIEGRIST, J. P. REMEIKA, E. A. RIETMAN, S. ZAHURAK and G. P. ESPINOSA, *Phys. Rev. Lett.* **58** (1987) 1676.
15. G. VAN TENDELOO, H. W. ZANDBERGEN and S. AMELINCKX, *Solid State Commun.* **63** (1987) 389.
16. Powder Diffraction File, International Center for Diffraction, Swarthmore, PA.
17. S. K. STREIFFER, B. M. LAIRSON, C. B. EOM, B. M. CLEMENS, J. C. BRAVMAN and T. H. GEBALLE, *Phys. Rev. B* **43** (1991) 3007.
18. L. A. TIETZ, C. B. CARTER, D. K. LATHROP, S. E. RUSSEK and R. A. BUHRMAN, in "High Temperature Superconductors" edited by M. B. Brodsky, R. C. Dynes, K. Kitazawa, and H. L. Tuller, Materials Research Society Symposium Proceedings, Vol. **99** (MRS, Pittsburgh PA, 1988) p. 715.
19. M. G. NORTON, L. A. TIETZ, C. B. CARTER, S. E. RUSSEK, B. H. MOECKLY and R. A. BUHRMAN, in "High Temperature Superconductors: Fundamental Properties and Novel Materials Processing", edited by J. Narayan, C. W. Chu, L. F. Schneemeyer, and D. K. Christen, Materials Research Society Symposium Proceedings, Vol. **169** (MRS, 1990) p. 513.
20. D. A. PORTER and K. E. EASTERLING, in "Phase Transformations in Metals and Alloys" (Van Nostrand, New York, 1981) pp. 142–50.
21. M. G. NORTON and C. B. CARTER, *J. Cryst. Growth* **110** (1991) 64.
22. R. RAMESH, D. HWANG, T. S. RAVI, A. INAM, J. B. BARNER, L. NAZAR, S.-W. CHAN, C. Y. CHEN, B. DUTTA, T. VENKATESAN and X. D. WU, *Appl. Phys. Lett.* **56** (1990) 2243.
23. D. A. SMITH, M. F. CHISHOLM and J. CLABES, *ibid.* **53** (1988) 2344.
24. J. W. EDINGTON, in "Practical Electron Microscopy in Materials Science Monograph 3: Interpretation of Transmission Electron Micrographs" (MacMillan Philips Technical Library, Eindhoven, 1975) pp. 80–4.
25. L. A. TIETZ, C. B. CARTER, D. K. LATHROP, S. E. RUSSEK, R. A. BUHRMAN and J. R. MICHAEL, *J. Mater. Res.* **4** (1989) 1072.

26. D. W. PASHLEY, in "Thin Films" (American Society of Metals, Metals Park, OH, 1964) pp. 59–98.
27. F. R. N. NABARRO, in "Theory of Crystal Dislocations" (Dover, New York, 1987) p. 303.
28. M. G. NORTON and C. B. CARTER, in "Proceedings of the Electron Microscopy Society of America", 50th Annual Meeting, edited by G. W. Bailey, J. Bentley and J. A. Small (San Francisco Press, San Francisco, CA, 1992) p. 236.
29. J. GEERK, G. LINKER and O. MEYER, *Mater. Sci. Rep.* **4** (1989) 193.
30. S. J. PENNYCOOK, M. F. CHISHOLM, D. E. JESSON, R. FEENSTRA, S. ZHU, X. Y. ZHENG and D. J. LOWNDES, *Phys. C* **202** (1992) 1.
31. U. DAHMEN, C. J. D. HETHERINGTON and K. H. WESTMACOTT, in "Proceedings of the XIIth International Congress for Electron Microscopy", edited by L. D. Peachey and D. B. Williams (San Francisco Press, San Francisco, CA, 1990) p. 338.
32. H. P. LANG, T. FREY and H.-J. GÜNTHERODT, *Europhys. Lett.* **15** (1991) 667.
33. M. G. NORTON and C. B. CARTER, *Phys. C* **182** (1991) 30.
34. D. G. SCHLOM, D. ANSELMETTI, J. G. BEDNORZ, R. F. BROOM, A. CATANA, T. FREY, Ch. GERBER, H.-J. GÜNTHERODT, H. P. LANG and J. MANNHART, *Z. Phys. B* **86** (1992) 163.
35. D. P. NORTON, D. H. LOWNDES, X.-Y. ZHENG, S. ZHU and R. J. WARMACK, *Phys. Rev. B Rapid Commun.* **44** (1991) 9760.

Received 30 September 1993
and accepted 9 June 1994